PAPER

Check for updates

Asymmetric sky-blue thermally-activated delayed fluorescence emitters bearing tris(triazolo)triazine moiety for solution-processable organic light-emitting diodes†

Zhou Fang,[a] Shengyue Wang,[a] Junxu Liao,[b] Xinrui Chen,[a] Yuanyuan Zhu,[a] Weiguo Zhu ⓘD *[a] and Yafei Wang ⓘD *[a]

An efficient blue thermally-activated delayed fluorescence (TADF) emitter is still a challenge in solution-processed organic light-emitting diodes (OLEDs). In this contribution, two asymmetric molecules, **TTT-Ac** and **TTT-2Ac** were synthesized and characterized, in which the tris(triazolo)triazine (TTT) fragment is used as the acceptor core and different numbers of acridine (Ac, one or two) units are considered as the donor unit. Both compounds display clear TADF character, concomitant with the emission between 420 and 450 nm in a doped PMMA film. Compared to **TTT-2Ac**, **TTT-Ac** shows blue-shifted emission due to its weaker intramolecular charge transfer effect. The solution-processed OLEDs achieve a maximum external quantum efficiency (EQE_{max}) of 9.26% and 8.10% with the emission peak at about 470 nm for **TTT-Ac** and **TTT-2Ac**, respectively. Furthermore, the **TTT-Ac**-based solution-processed OLED exhibits an EQE_{max} of 10.01% after optimization of the emitter thickness. This research focuses on the molecular structure–property relationship of TTT-based molecules, which enriches the TTT-based solution-processable sky-blue TADF emitter.

Introduction

Since the first example of an organic thermally-activated delayed fluorescent (TADF) material was utilized in organic light-emitting diodes (OLEDs) by Adachi's research group,[1] organic TADF materials have attracted considerable interest from both academe and industry due to their high efficiency and metal-free atoms.[2,3] Compared with traditional organic fluorescent materials, TADF materials can harvest both singlet and triplet excitons through the reverse intersystem crossing process, leading to theoretical 100% internal quantum efficiency.[4–7] In addition, metal atoms are absent from organic TADF materials, making them definitely low-cost and eco-friendly relative to phosphorescent materials.[8–10] According to previous reports,[11–15] the prerequisite for constructing a TADF molecule is to achieve a small energy splitting (ΔE_{ST}) between singlet (S_1) and triplet (T_1) excited states, which usually is

realized *via* minimizing the spatial overlap between the highest occupied molecular orbitals (HOMO) and lowest unoccupied molecular orbitals (LUMO).

To this end, the most effective strategy for TADF materials is to design a twisted molecule with a donor–acceptor/donor–π–acceptor (D–A/D–π–A) skeleton.[16–21] This molecular structure can effectively separate the HOMO and LUMO, thus reducing the energy gap between S_1 and T_1 states. Therefore, many high-efficiency TADF emitters have been developed based on D–A/D–π–A systems, and their external quantum efficiencies (EQEs) in OLEDs exceed 20%.[22–29] Unfortunately, blue TADF emitters still lag far behind green and red ones because of the bathochromic shift in the D–A/D–π–A molecules caused by strong intramolecular charge transfer (ICT). Thus, how to balance ICT and blue emission is very important for blue TADF emitters. Recently, some effective methods to achieve blue TADF emitters have been reported, such as decreasing the conjugation degree, utilization of a weak acceptor and realizing multiresonant-TADF.[30–33] Although certain blue TADF emitters have obtained excellent efficiency in devices,[34–37] the vast majority of them are prepared *via* full vapor deposition, involving complicated fabrication procedures and high cost. In addition, the reported blue TADF emitters usually contain an acceptor with low-rigidity structure, such as triazine, triphenyl boron, diphenyl sulphone fragments,[38–43] which is not beneficial to suppress

[a] *Jiangsu Collaborative Innovation Center of Photovoltaic Science and Engineering, Jiangsu Engineering Laboratory of Light-Electricity-Heat Energy-Converting Materials and Applications, School of Materials Science & Engineering, Changzhou University, Changzhou 213164, China. E-mail: zhuwg18@126.com, qiji830404@hotmail.com*

[b] *School of Chemical Engineering and Energy Technology, Dongguan University of Technology, Dongguan, 523808, China*

† Electronic supplementary information (ESI) available. See DOI: 10.1039/d1tc05372h

This journal is © The Royal Society of Chemistry 2022

J. Mater. Chem. C, 2022, **10**, 4837–4844 | **4837**

the molecular deformation in the excited state. Therefore, there is much space to develop novel blue TADF emitters for solution-processable OLEDs.

The tristriazolotriazine (TTT) moiety is a polyazin, which is a popular candidate in liquid crystal studies due to its rigid and planar structure.[44,45] Impressively, this fragment was employed as an acceptor group in blue TADF emitters by Yang, Eli and our groups at the same time (Fig. S1, ESI†).[46–48] These researches demonstrated that the TTT unit possesses moderate electron-withdrawing ability and high molecular rigidity, which can be employed as an acceptor in blue TADF emitters. After optimizing the device, we recently reported the sky-blue TADF emitter of TTT-Ph-Ac with a highest EQE of 22% in a solution-processed OLED.[49] However, the electroluminescent (EL) emission is at about 490 nm, not the real blue region. Very recently, Hojo *et al.* also reported a green TADF emitter based on a TTT core (Fig. S1, ESI†).[50] Unfortunately, the device performance of these emitters was not reported. It is worth noting that all these TTT-based emitters are symmetric molecules with three donor groups, probably a simple synthetic method. As is known, decreasing the number of donor units can effectively reduce the ICT effect, and then lead to a hypochromic shift. With this in mind, the proposal to prepare asymmetric emitters based on TTT acceptor with one or two donor units was made to realize blue emission. Herein, two TTT-based emitters, named **TTT-Ac** and **TTT-2Ac**, with one and two acridine (Ac) moieties, respectively, were synthesized and characterized. As expected, both emitters showed blue-shifted emission in solution and film compared to the TTT-based TADF material with three Ac fragments. A solution-processable device employing **TTT-Ac** as the emitter achieved a maximum EQE of 10.01% with the EL emission peak at 474 nm.

Results and discussion

Materials and thermal properties

As shown in Scheme 1, starting from the commercial materials of 2,4,6-trichloro-1,3,5-triazine, 5-(4-bromobenzene)-1*H*-tetrazole and 5-phenyltetrazole, the key precursors of TTT-Br and TTT-2Br were prepared by a one-pot Huisgen reaction in a yield of 25% and 38%, respectively. Then, a Buchwald–Hartwig coupling reaction between TTT-Br/TTT-2Br and Ac provided the target TADF emitters (**TTT-Ac** and **TTT-2Ac**) in the presence of Pd catalyst, which was evidenced by ^{1}H NMR, ^{13}C NMR, TOF-MS and HRMS (Fig. S2–S11, ESI†). Both compounds exhibited good solubility in ordinary organic solvents, such as toluene, CH_2Cl_2, $CHCl_3$ and THF. Impressively, excellent thermal stability was found, with the decomposition temperature (T_d, at 5 wt% weight loss) determined to be 415 and 417 °C for **TTT-Ac** and **TTT-2Ac**, respectively (Fig. S12, ESI†).

Theoretical calculations

To better explore the geometric configurations and frontier molecular orbital energy levels of both emitters, density functional theory simulations were conducted based on Gaussian 09 program (b3lyp/6-31g(d)). As shown in Fig. 1, both emitters show a twisted molecular configuration, in which large spatial separations between HOMO and LUMO were observed from orbital pictures. The LUMOs of both compounds are mainly distributed on the TTT acceptor, while the HOMO distributions are mainly governed by the donor units. It is notable that HOMOs and LUMOs of both molecules are weakly overlapped at the bridged phenyl ring, indicating the possibility of high emission efficiency. The theoretical ΔE_{ST} values (energy gap between singlet and triplet energies) are evaluated to be 0.0071 for **TTT-Ac** and 0.0068 for **TTT-2Ac**. Such small ΔE_{ST} values are very conducive to reverse intersystem crossing from T_1 to S_1. The small ΔE_{ST} can be assigned to the vertical twist between the donor and bridged phenyl ring caused by strong electron-donating ability of the Ac unit according to our previous work. However, the amount of donor moieties seems to have less influence in the distribution of HOMO and LUMO. In conclusion, both molecules have separated distribution of HOMO and LUMO while being slightly overlapped at bridged phenyl ring, which may demonstrate great TADF characteristics.
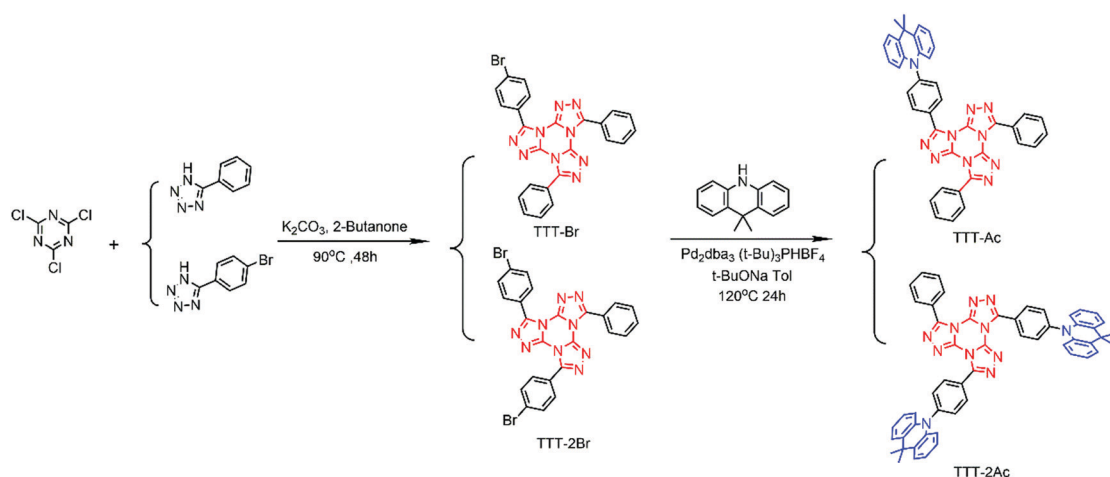
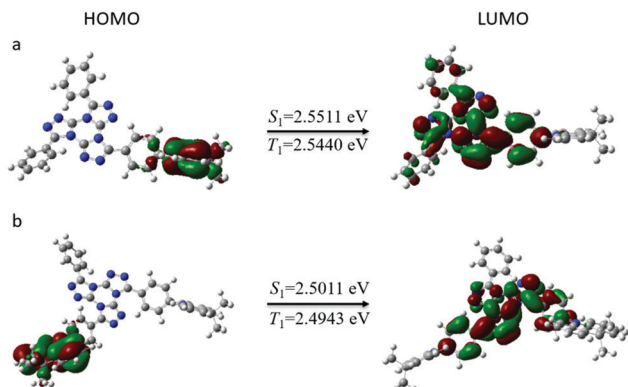Scheme 1 Synthetic route of the TADF emitters.

Fig. 1 The calculated HOMO and LUMO distributions, and singlet and triplet energies of the compounds: (a) **TTT-Ac** and (b) **TTT-2Ac**.

Photophysical properties

The ultraviolet-visible (UV-vis) absorption and photoluminescence (PL) spectra in both toluene solution and doped PMMA films at room temperature are depicted in Fig. 2, and the relevant data are listed in Table 1. Both emitters exhibit similar absorption spectra with two clear absorption bands from 250 nm to 400 nm (Fig. 2a). The intense absorption bands at 283 nm are assigned to the $\pi-\pi^*$ transition of the aromatic backbone, while the weak absorption bands at about 355 nm are ascribed to the ICT from the donor to the acceptor units. It is worth noting that there is a slightly red-shifted absorption band for **TTT-2Ac** compared to that for **TTT-Ac** due to the stronger ICT effect caused by one more donor unit.

At an excitation wavelength of 350 nm, the PL spectra with emission peaks at 468 and 471 nm are observed in dilute toluene solution for **TTT-Ac** and **TTT-2Ac** (Fig. 2b), respectively. Compared to our previous reports,[51] this result demonstrates that decreasing the number of donor moieties effectively leads to blue-shifted emission owing to a reduced ICT effect. The broad and structureless shape of the PL profiles implies that the emission is mainly generated from the charge transfer (CT) state. In addition, the solvent-dependent emission spectra (Fig. S13, ESI†) also point to there being a strong CT state in both emitters, evidenced by the clear solvatochromism effect.

Fig. 2 UV-Vis spectra (a) and PL spectra measured in toluene solution (b) and PL spectra in doped PMMA film (c) at room temperature.

Table 1 Photophysical data of compounds **TTT-Ac** and **TTT-2Ac**

Compound	$\lambda_{abs}{}^a$/ nm	$\lambda_{em}{}^a$/ nm	$\lambda_{em}{}^b$/ nm	$\tau_p{}^b$/ ns	$\Phi_p{}^b$/ %	$\tau_d{}^b$/ μs	$\Phi_d{}^b$/ %	$\Phi_{total}{}^b$/ %	$T_d{}^c$/ °C	E_g^{opt}
TTT-Ac	283, 353	468	426	10.9	21	27.2	42	63	415	2.99
TTT-2Ac	283, 355	471	446	11.9	10	20	37	47	413	2.96

[a] In toluene at room temperature. [b] 10 wt% in PMMA at room temperature. [c] In N_2 at a heating rate of 20 °C min^{-1}.

Compared to solution, the doped PMMA films exhibit a blue shift with emission peaks at 426 and 446 nm for **TTT-Ac** and **TTT-2Ac**, respectively (Fig. 2c). Two factors could be responsible for this phenomenon: (i) the suppressed molecular motions in the solid state; and (ii) and the polarity of the PMMA film.[51] Owing to the stronger ICT effect, compound **TTT-2Ac** shows distinct red-shifted emission spectra compared with **TTT-Ac** in both solution and film. Impressively, a shoulder at about 380 nm is detected for **TTT-Ac**, which can be attributed to emission from a localized state of the Ac unit.[52]

The low-temperature (77 K) fluorescence and phosphorescence spectra of both emitters were measured in doped PMMA (10 wt%) film (Fig. 3a and b). According to the onsets of fluorescence and phosphorescence spectra, the S_1/T_1 energy levels were evaluated to be 3.19/2.84 eV for **TTT-Ac** and 3.09/2.9 eV for **TTT-2Ac**. Therefore, the corresponding ΔE_{ST} values were calculated to be 0.35 eV (**TTT-Ac**) and 0.19 eV (**TTT-2Ac**). The smaller ΔE_{ST} of **TTT-2Ac** was attributed to its stronger ICT effect. To verify the TADF characteristics of the emitters, the transient PL decay profiles were measured in doped PMMA films at room temperature. Both emitters showed double-exponential decay curves consisting of prompt and delayed components. The lifetimes of prompt/delayed components were 1.89 ns/44.79 μs for **TTT-Ac** and 10.04 ns/34.6 μs for **TTT-2Ac**. Both the small ΔE_{ST} values and the delayed components indicate the participation of the triplet exciton through the reverse intersystem crossing process. The PL quantum yields (PLQYs) of the two emitters in doped PMMA films were measured to be 63% and 47% for **TTT-Ac** and **TTT-2Ac**, respectively. Based on the PLQY and lifetime, the photophysical constants, such as the rate constants of fluorescence (k_r), nonradiative transition (k_{nr}), intersystem crossing (k_{ISC}) and reverse intersystem crossing (k_{rISC}), were calculated according to a previous method (formulas S(1)–S(6) and Table S1, ESI†). Compared to **TTT-Ac**, compound **TTT-2Ac** exhibits a higher k_{rISC} of 2.055×10^5 s^{-1}, probably due to the smaller ΔE_{ST} and multiple channels. Unfortunately, relatively slow k_r and large k_{nr} are determined for **TTT-2Ac**, leading to a small emission efficiency.

Electrochemical properties

To investigate the electrochemical properties, cyclic voltammetry measurements were performed on the neat film in degassed CH_3CN solution (0.1 M). As shown in Fig. S14 (ESI†), an obvious oxidation process was observed with reversible oxidation potentials at 0.95 and 0.68 V for **TTT-Ac** and **TTT-2Ac**, respectively.

Fig. 3 PL spectra of **TTT-Ac** (a) and **TTT-2Ac** (b) in 10 wt%-doped PMMA film at 77 K and transient PL prompt (inset) and delayed curves in 10 wt%-doped PMMA films at room temperature (c and d).

Table 2 EL data for the devices

Material	Dopant/wt%	V_{ON}/V	L_{max}/cd m^{-2}	CE_{max}/cd A^{-1}	EQE_{max}/%	CIE (x, y)	Peak/nm
TTT-Ac	10	4.0	734.9	14.64	8.60	(0.16, 0.19)	468
	20	3.6	1078	16.21	9.26	(0.16, 0.21)	470
	30	3.6	1205	13.44	7.33	(0.16, 0.23)	474
TTT-2Ac	10	4.8	1011	13.45	7.04	(0.16, 0.24)	474
	20	3.6	1384	16.61	8.10	(0.17, 0.26)	474
	30	3.6	1395	10.10	4.79	(0.18, 0.30)	482

The HOMO energy levels were -5.29 and -5.13 eV for **TTT-Ac** and **TTT-2Ac** according to the empirical formula of $E_{HOMO} = -(V_{OX} - V_{Fc/Fc^+} + 4.8)$ eV. Compared to **TTT-Ac**, **TTT-2Ac** shows a shallow HOMO level due to its stronger electron-donating ability. The LUMO energy levels were calculated to be -2.3 and -2.17 eV for **TTT-Ac** and **TTT-2Ac** based on their HOMO levels and optical bandgaps.

Electroluminescent properties

To further explore the EL properties of both compounds, **TTT-Ac** and **TTT-2Ac** were used as dopants in solution-processed OLEDs with a device configuration of ITO/PEDOT:PSS (40 nm)/mCP:EML (X wt%, X = 10, 20, 30) (30 nm)/DPEPO (9 nm)/TmPyPB (45 nm)/LiF (0.5 nm)/Al (120 nm). The emitting layer is a blend of mCP and **TTT-Ac** or **TTT-2Ac** with different dopant concentrations of 10, 20 and 30 wt%. Schematic diagrams of the energy levels and chemical structures of materials in the

devices are shown in Fig. S15(ESI†), and the relevant data are listed in Table 2.

As shown in Fig. 4, both emitters show sky-blue emissions in the devices, and their CIE (Commission International de l'Eclairage) coordinates vary from (0.16, 0.19) to (0.18, 0.30) (Fig. S16, ESI†). Similar to the PL profiles, the **TTT-Ac**-based devices exhibit blue-shifted emission relative to the **TTT-2Ac**-based devices. On the other hand, the host emission peaks are absence from the EL spectra, implying the complete energy transfer from mCP to the dopant.

As seen from the current density–voltage–luminance (J–V–L) curves, both current density and luminance are increased with increasing dopant concentration, suggesting a charge trapping mechanism in the devices. Both the emitters exhibit the best device performance at 20 wt% dopant concentration. The turn-on voltage (V_{on} at 1 cd m^{-2}) and maximum luminescence were 3.6 V/1205 cd m^{-2} and 3.6 V/1395 cd m^{-2} for

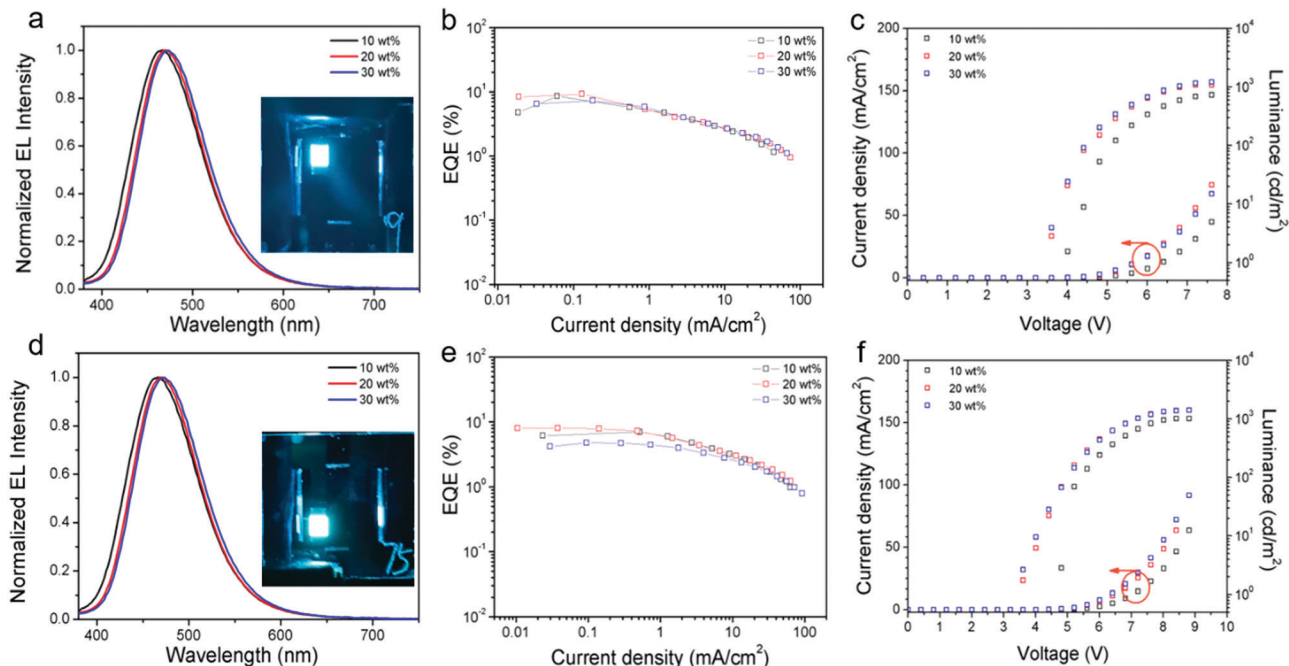**4840** | *J. Mater. Chem. C*, 2022, **10**, 4837–4844

This journal is © The Royal Society of Chemistry 2022

Fig. 4 EL spectra (a) (inset: emission picture of the device); EQE−current density curves (b); and current density−voltage−luminance (J−V−L) curves (c) of **TTT-Ac**. EL spectra (d) (inset: emission picture of the device); EQE−current density curves (e); and current density−voltage−luminance (J−V−L) curves (f) of **TTT-2Ac**.
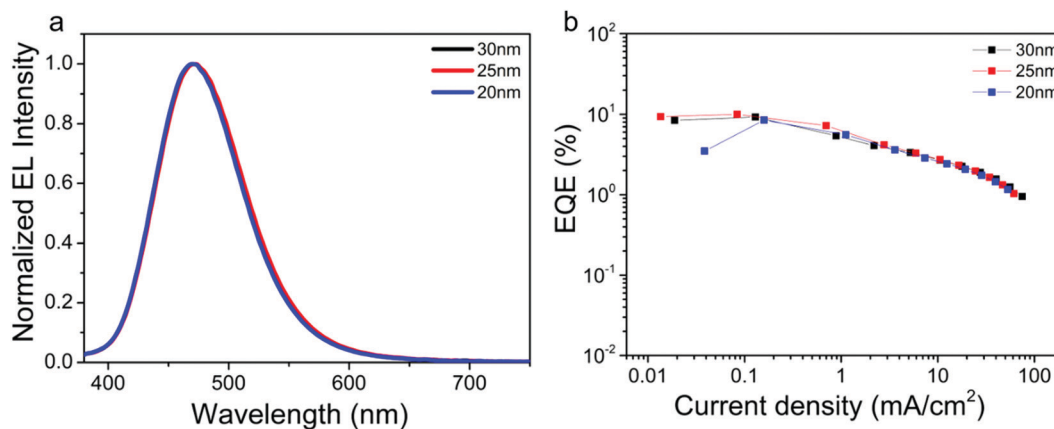

Fig. 5 EL spectra (a) and EQE−current density curves (b) of **TTT-Ac** with different EML thickness of 20 wt% dopants.

TTT-Ac- and **TTT-2Ac**-based devices, respectively. Owing to the higher PLQY, the **TTT-Ac**-based device achieved a better performance with maximum current efficiency (CE) of 16.21 cd A^{-1} and EQE of 9.26%, while devices based on **TTT-2Ac** achieved a maximum CE of 16.61 cd A^{-1} and EQE of 8.10%.

Based on our previous report,[49] the emitter layer thickness plays a key role in the device performance. Herein, taking **TTT-Ac** as an example, the influence of emitter layer thickness on the device performance is explored. The solution-processed devices with the same configuration of ITO/PEDOT:PSS (40 nm)/mCP:EML (X nm, X = 20, 25 and 30 nm)/DPEPO (9 nm)/TmPyPB (45 nm)/LiF (0.5 nm)/Al (120 nm) were fabricated, and the performance data of the devices are summarized in Fig. 5 and Fig. S17, Table S2 (ESI†).

As expected, the devices showed the best performance with 25 nm EML layer, concomitant with the maximum CE of 17.37 cd A^{-1} and EQE of 10.01%. This phenomenon could be ascribed to the balanced hole and electron currents influenced by the thickness of the emitter layer.[53] Compared to the reported TTT-based TADF emitters (Fig. S1 and S18, ESI†), **TTT-Ac** shows the bluest emission with high efficiency in solution-processable OLED.

Conclusion

In conclusion, two sky-blue TADF emitters, **TTT-Ac** and **TTT-2Ac**, were prepared by combining the electron acceptor of TTT and one or two Ac fragments. The influence of the donor

This journal is © The Royal Society of Chemistry 2022

J. Mater. Chem. C, 2022, **10**, 4837–4844 | **4841**

number on the photophysical properties was investigated in detail. The HOMO and LUMO of the two compounds were spatially separated, leading to small ΔE_{ST}. Intense deep blue emissions in doped films were obtained with PLQYs of 63% (426 nm) for **TTT-Ac** and 47% (446 nm) for **TTT-2Ac**. The solution-processed OLEDs based on **TTT-Ac** and **TTT-2Ac** achieved maximum EQEs of 9.26% at 470 nm and 8.10% at 474 nm, respectively. Furthermore, by optimizing the emitter layer thickness, the **TTT-Ac**-based solution-processed OLEDs exhibited a maximum EQE of 10.01%. This work provided a novel method for designing sky-blue emitters for solution-processed OLEDs.

Experimental section

General procedure for synthesis

Synthesis of compounds TTT-Br and TTT-2Br. A mixture of 5-(4-bromobenzene)-1H-tetrazole (1.2 g, 5.43 mmol), 5-phenyltetrazole (1.75 g, 11.95 mmol), 2,4,6-trichloro-1,3,5-triazine (1.0 g, 5.43 mmol), anhydrous potassium carbonate (9.0 g, 65.16 mmol) and 100 mL 2-butanone was heated to 90 °C under dry air conditions and refluxed for 48 h. After completion of the reaction, 2-butanone was removed by vacuum distillation; residual inorganic salts and water-soluble impurities were washed with water and then the reaction mixture was dried. The remaining mixture was dissolved in dichloromethane and then dried with silica gel particles. 600 mg of compound TTT-Br and 500 mg of compound TTT-2Br were obtained by column chromatography using dichloromethane as an eluent, both as white powders.

TTT-Br. ^{1}H NMR (500 MHz, CDCl$_3$) δ (ppm) 8.14–8.10 (m, 2H), 8.05 (t, J = 8.8 Hz, 4H), 7.75 (dd, J = 8.7, 2.4 Hz, 4H), 7.67 (t, J = 7.4 Hz, 1H), 7.61 (t, J = 7.4 Hz, 2H).

TTT-2Br. ^{1}H NMR (500 MHz, CDCl$_3$) δ (ppm) 8.14–8.10 (m, 2H), 8.05 (t, J = 8.8 Hz, 4H), 7.75 (dd, J = 8.7, 2.4 Hz, 4H), 7.67 (t, J = 7.4 Hz, 1H), 7.61 (t, J = 7.4 Hz, 2H) (Fig. S1 and S2, ESI†).

Synthesis of compound TTT-Ac. A mixture of compound TTT-Br (120 mg, 0.236 mmol), 9,10-dihydro-9,9-dimethylacridine (99 mg, 0.472 mmol), tris(dibenzylideneacetone)dipalladium (13 mg, 0.014 mmol), tri-*tert*-butylphosphonium tetrafluoroborate (8.3 mg, 0.028 mmol), sodium *tert*-butoxide (91 mg, 0.944 mmol) and 25 mL toluene was heated to 120 °C and refluxed for 24 h under the protection of nitrogen. After the reaction, it was cooled to room temperature, toluene was removed by vacuum distillation, water-soluble impurities were removed by washing (50 mL) the remaining reactants, and residual solvents were removed by drying and vacuum distillation. The residue was separated by column chromatography with petroleum ether : dichloromethane (1 : 1) as eluent to afford white solid (60 mg, yield 40%). ^{1}H NMR (400 MHz, CDCl$_3$) δ (ppm) 8.46 (d, J = 8.5 Hz, 2H), 8.19–8.15 (m, 4H), 7.71–7.58 (m, 9H), 7.49 (dd, J = 7.6, 1.4 Hz, 2H), 7.07–6.95 (m, 5H), 6.43 (d, J = 7.1 Hz, 2H), 1.71 (s, 6H). ^{13}C NMR (126 MHz, CDCl$_3$) δ (ppm) 151.00 (d, J = 15.1 Hz), 150.42, 143.64, 141.77, 140.67, 138.57, 132.08, 131.78, 130.20, 128.68, 126.07, 123.91, 121.64, 116.36, 109.47, 34.80, 32.00. TOF-MS (ESI) m/z calcd for C$_{39}$H$_{28}$N$_{10}$ [M + H]$^+$: 637.72; found: 637.29; HRMS (ESI) m/z found: 637.256144 C$_{39}$H$_{28}$N$_{10}$ (Fig. S4, S6, S8 and S10, ESI†).

Synthesis of compound TTT-2Ac. A mixture of compound TTT-2Br (120 mg, 0.204 mmol), 9,10-dihydro-9,9-dimethyl-acridine (171 mg, 0.817 mmol), tris(dibenzylideneacetone)dipalladium (11.2 mg, 0.012 mmol), tri-*tert*-butylphosphonium tetrafluoroborate (7.1 mg, 0.025 mmol), sodium *tert*-butoxide (78 mg, 0.817 mmol) and 50 mL toluene was heated to 120 °C under the protection of nitrogen and refluxed for 24 h. After the reaction, it was cooled to room temperature, toluene was removed by vacuum rotary distillation, the remaining reactants were washed with water (50 mL) to remove water-soluble impurities, dried, and the residual solvent was removed by vacuum distillation. The residue was separated by column chromatography with petroleum ether : dichloromethane (1 : 1) as eluent to afford yellow solid (70 mg, yield 40%). ^{1}H NMR (400 MHz, CDCl$_3$) δ (ppm) 8.48 (dd, J = 8.5, 2.7 Hz, 4H), 8.22–8.17 (m, 2H), 7.71–7.60 (m, 7H), 7.50 (d, J = 7.6 Hz, 4H), 7.08–7.02 (m, 4H), 6.99 (t, J = 7.4 Hz, 4H), 6.47–6.42 (m, 4H), 1.71 (s, 12H). ^{13}C NMR (126 MHz, CDCl$_3$) δ (ppm) 151.16, 150.47, 145.00, 140.85, 132.81, 132.19, 131.32, 130.73, 130.22, 128.76, 126.53, 125.31, 123.77, 123.40, 121.17, 114.56, 36.12, 31.04. TOF-MS (ESI) m/z calcd for C$_{54}$H$_{41}$N$_{11}$ [M + H]$^+$: 844.00; found: 844.348. HRMS (ESI) m/z found: 844.360839, C$_{54}$H$_{42}$N$_{11}$ (Fig. S5, S7, S9 and S11, ESI†).

Fabrication and measurements of OLED device

Solution-processed device. Poly(styrene sulfonate) (PEDOT:PSS) was purchased from Xi'an Polymer Light Technology Corp. 9,9′-(1,3-Phenylene)bis-9H-carbazole (mCP), bis(2-(diphenylphosphino)phenyl) ether oxide (DPEPO), 1,3,5-tri(m-pyrid-3-ylphenyl)benzene (TmPyPB), and LiF were purchased from Lumtec. All commercially available reagents were used without further purification. In devices, PEDOT:PSS was used as hole injection material. mCP was chosen as host material and DPEPO was used as hole blocking material. TmPyPB and LiF were used as electron transport and injection materials, respectively. ITO (indium tin oxide) and Al (aluminum) were used as anode and cathode materials, respectively.

The substrates were successively cleaned with isopropyl alcohol, acetone, detergent, deionized water, and isopropyl alcohol in an ultrasonic bath and then dried overnight in an oven. The substrates were pre-treated with oxygen plasma to increase the work function of the ITO film. Then, 40 nm-thick PEDOT:PSS was spin-coated onto the ITO substrates at 3200 rpm for 30 s and annealed at 150 °C for 15 min. And then emissive layer was spin-coated and annealed at 60 °C or 110 °C for 30 min using a precursor containing different materials co-dissolved in chlorobenzene or toluene. The films of DPEPO, TmPyPB, LiF and aluminum were prepared by thermal evaporation under a vacuum of 1×10^{-4} Pa. Each sample had an active area of 0.04 cm^2.

All the devices were encapsulated before characterization to prevent degradation and emission quenching caused by oxygen and water. The EL spectra and J–V–R curves were obtained with a Photoresearch Spectra Scan PR735 photometer and a Keithley 2400 source meter constant current source at room temperature. The EQE values were calculated by assuming a Lambertian distribution.

Conflicts of interest

There are no conflicts to declare.

4842 | *J. Mater. Chem. C*, 2022, **10**, 4837–4844

This journal is © The Royal Society of Chemistry 2022

Acknowledgements

References

1 K. Goushi and C. Adachi, *Appl. Phys. Lett.*, 2012, **101**, 023306.

2 Y. Zou, S. Gong, G. Xie and C. Yang, *Adv. Opt. Mater.*, 2018, **6**, 1800568.

3 G. Hong, X. Gan, C. Leonhardt, Z. Zhang, J. Seibert, J. M. Busch and S. Brase, *Adv. Mater.*, 2021, **33**, 2005630.

4 Z. Yang, Z. Mao, Z. Xie, Y. Zhang, S. Liu, J. Zhao, J. Xu, Z. Chi and M. P. Aldred, *Chem. Soc. Rev.*, 2017, **46**, 915–1016.

5 S. K. Jeon, H. L. Lee, K. S. Yook and J. Y. Lee, *Adv. Mater.*, 2019, **31**, 1803524.

6 X. Liang, Z. L. Tu and Y. X. Zheng, *Chem. – Eur. J.*, 2019, **25**, 5623–5642.

7 Y. Tao, K. Yuan, T. Chen, P. Xu, H. Li, R. Chen, C. Zheng, L. Zhang and W. Huang, *Adv. Mater.*, 2014, **26**, 7931–7958.

8 P. Ganesan, W. Y. Hung, J. Y. Tso, C. L. Ko, T. H. Wang, P. T. Chen, H. F. Hsu, S. H. Liu, G. H. Lee, P. T. Chou, A. K. Y. Jen and Y. Chi, *Adv. Funct. Mater.*, 2019, **29**, 1900923.

9 S. Tan, X. Wu, Y. Zheng and Y. Wang, *Chin. Chem. Lett.*, 2019, **30**, 1951–1954.

10 Z. Wei, K. Zhang, C. K. Kim, S. Tan, S. Wang, L. Wang, J. Li and Y. Wang, *Chin. Chem. Lett.*, 2021, **32**, 493–496.

11 M. Godumala, S. Choi, M. J. Cho and D. H. Choi, *J. Mater. Chem. C*, 2016, **4**, 11355–11381.

12 T. Huang, W. Jiang and L. Duan, *J. Mater. Chem. C*, 2018, **6**, 5577–5596.

13 M. Y. Wong and E. Zysman-Colman, *Adv. Mater.*, 2017, **29**, 1605444.

14 J. H. Kim, J. H. Yun and J. Y. Lee, *Adv. Opt. Mater.*, 2018, **6**, 1800255.

15 Y. Im, M. Kim, Y. J. Cho, J.-A. Seo, K. S. Yook and J. Y. Lee, *Chem. Mater.*, 2017, **29**, 1946–1963.

16 J. M. Teng, Y. F. Wang and C. F. Chen, *J. Mater. Chem. C*, 2020, **8**, 11340–11353.

17 Q. Xue and G. Xie, *Adv. Opt. Mater.*, 2021, **9**, 2002204.

18 W. Che, Y. Xie and Z. Li, *Asian J. Org. Chem.*, 2020, **9**, 1262–1276.

19 M. Godumala, S. Choi, M. J. Cho and D. H. Choi, *J. Mater. Chem. C*, 2019, **7**, 2172–2198.

20 X. Cao, D. Zhang, S. Zhang, Y. Tao and W. Huang, *J. Mater. Chem. C*, 2017, **5**, 7699–7714.

21 D. G. Chen, T. C. Lin, C. L. Chen, Y. T. Chen, Y. A. Chen, G. H. Lee, P. T. Chou, C. W. Liao, P. C. Chiu, C. H. Chang, Y. J. Lien and Y. Chi, *ACS Appl. Mater. Interfaces*, 2018, **10**, 12886–12896.

22 T. Yang, Z. Cheng, Z. Li, J. Liang, Y. Xu, C. Li and Y. Wang, *Adv. Funct. Mater.*, 2020, **30**, 2002681.

23 Z. Li, D. Yang, C. Han, B. Zhao, H. Wang, Y. Man, P. Ma, P. Chang, D. Ma and H. Xu, *Angew. Chem., Int. Ed.*, 2021, **60**, 14846–14851.

24 F.-M. Xie, Z.-D. An, M. Xie, Y.-Q. Li, G.-H. Zhang, S.-J. Zou, L. Chen, J.-D. Chen, T. Cheng and J.-X. Tang, *J. Mater. Chem. C*, 2020, **8**, 5769–5776.

25 J. Jin, H. Jiang, Q. Yang, L. Tang, Y. Tao, Y. Li, R. Chen, C. Zheng, Q. Fan, K. Y. Zhang, Q. Zhao and W. Huang, *Nat. Commun.*, 2020, **11**, 842.

26 R. Braveenth, H. Lee, J. D. Park, K. J. Yang, S. J. Hwang, K. R. Naveen, R. Lampande and J. H. Kwon, *Adv. Funct. Mater.*, 2021, 2105805.

27 Y. K. Chen, J. Jayakumar, C. M. Hsieh, T. L. Wu, C. C. Liao, J. Pandidurai, C. L. Ko, W. Y. Hung and C. H. Cheng, *Adv. Mater.*, 2021, **33**, 2008032.

28 H. J. Park, H. L. Lee, H. J. Lee, K. H. Lee, J. Y. Lee and W. P. Hong, *Chem. Mater.*, 2019, **31**, 10023–10031.

29 X. Liang, Z. P. Yan, H. B. Han, Z. G. Wu, Y. X. Zheng, H. Meng, J. L. Zuo and W. Huang, *Angew. Chem., Int. Ed.*, 2018, **57**, 11316–11320.

30 X. Cai and S.-J. Su, *Adv. Funct. Mater.*, 2018, **28**, 1802558.

31 X. Zheng, R. Huang, C. Zhong, G. Xie, W. Ning, M. Huang, F. Ni, F. B. Dias and C. Yang, *Adv. Sci.*, 2020, **7** 1902087.

32 W. Li, W. Li, L. Gan, M. Li, N. Zheng, C. Ning, D. Chen, Y. C. Wu and S. J. Su, *ACS Appl. Mater. Interfaces*, 2020, **12**, 2717–2723.

33 H. Abroshan, Y. Zhang, X. Zhang, C. Fuentes-Hernandez, S. Barlow, V. Coropceanu, S. R. Marder, B. Kippelen and J. L. Brédas, *Adv. Funct. Mater.*, 2020, **30**, 2005898.

34 J. Zhang, Q. Wei, N. Fei, M. Zhao, L. Xie, L. Cao, X. Zhang, G. Xie, T. Wang and Z. Ge, *ACS Appl. Mater. Interfaces*, 2021, **13**, 12305–12312.

35 R. K. Konidena, J. Lim and J. Y. Lee, *Chem. Eng. J.*, 2021, **416**, 129097.

36 J. H. Yun, K. H. Lee, J. Y. Lee and W. P. Hong, *Chem. Eng. J.*, 2021, **411**, 128550.

37 H. Yang, Q. Liang, C. Han, J. Zhang and H. Xu, *Adv. Mater.*, 2017, **29**, 1700553.

38 H. J. Kim, M. Godumala, S. K. Kim, J. Yoon, C. Y. Kim, H. Park, J. H. Kwon, M. J. Cho and D. H. Choi, *Adv. Opt. Mater.*, 2020, **8**, 1902175.

39 Y. Wada, S. Kubo and H. Kaji, *Adv. Mater.*, 2018, **30**, 1705641.

40 K. Wu, Z. Wang, L. Zhan, C. Zhong, S. Gong, G. Xie and C. Yang, *J. Phys. Chem. Lett.*, 2018, **9**, 1547–1553.

41 L. Zhan, Z. Chen, S. Gong, Y. Xiang, F. Ni, X. Zeng, G. Xie and C. Yang, *Angew. Chem., Int. Ed.*, 2019, **58**, 17651–17655.

42 J. Luo, S. Gong, Y. Gu, T. Chen, Y. Li, C. Zhong, G. Xie and C. Yang, *J. Mater. Chem. C*, 2016, **4**, 2442–2446.

43 I. H. Lee, W. Song, J. Y. Lee and S.-H. Hwang, *J. Mater. Chem. C*, 2015, **3**, 8834–8838.

44 T. Rieth, N. Roder, M. Lehmann and H. Detert, *Chem. – Eur. J.*, 2018, **24**, 93–96.

45 T. Rieth, T. Marszalek, W. Pisula and H. Detert, *Chem. – Eur. J.*, 2014, **20**, 5000–5006.

46 S. K. Pathak, Y. Xiang, M. Huang, T. Huang, X. Cao, H. Liu, G. Xie and C. Yang, *RSC Adv.*, 2020, **10**, 15523–15529.

47 F. Hundemer, E. Crovini, Y. Wada, H. Kaji, S. Bräse and E. Zysman-Colman, *Mater. Adv.*, 2020, **1**, 2862–2871.

48 S. Wang, X. Wang, K. H. Lee, S. Liu, J. Y. Lee, W. Zhu and Y. Wang, *Dyes Pigm.*, 2020, **182**, 108589.

49 X. Chen, S. Wang, H. L. Lee, J. Y. Lee, X. Liao, L. Li, W. Zhu and Y. Wang, *Adv. Opt. Mater.*, 2021, 2101518.

50 R. Hojo, D. M. Mayder and Z. M. Hudson, *J. Mater. Chem. C*, 2021, **9**, 14342–14350.

51 Y. Liu, Z. Yin, X. Wang, E. Baranoff, D. Zhou, K. Zhang, Z. Ren, S. Wang, W. Zhu and Y. Wang, *J. Mater. Chem. C*, 2020, **8**, 8971–8979.

52 B. Li, Z. Yang, W. Gong, X. Chen, D. W. Bruce, S. Wang, H. Ma, Y. Liu, W. Zhu, Z. Chi and Y. Wang, *Adv. Opt. Mater.*, 2021, **9**, 2100180.

53 M. R. Fadavieslam, *Optik*, 2019, **182**, 452–457.

4844 | *J. Mater. Chem. C*, 2022, **10**, 4837–4844

This journal is © The Royal Society of Chemistry 2022